Supplementary Information

Electrochemically induced catalytic adsorption sites in spent lithium–ion battery cathodes for high–rate vanadium redox flow battery

Jeongmok Park,‡[a] Hongsoo Jin,‡[a] Minseong Kim,[a] Haeseong Jang,*[b] and Minseong Ko*[a]

[a]Metallurgical Engineering, Pukyong National University, Busan 48547, Republic of Korea

[b]Beamline Research Division Pohang Accelerator Laboratory, Pohang University of Science and Technology (POSTECH), Pohang, Republic of Korea

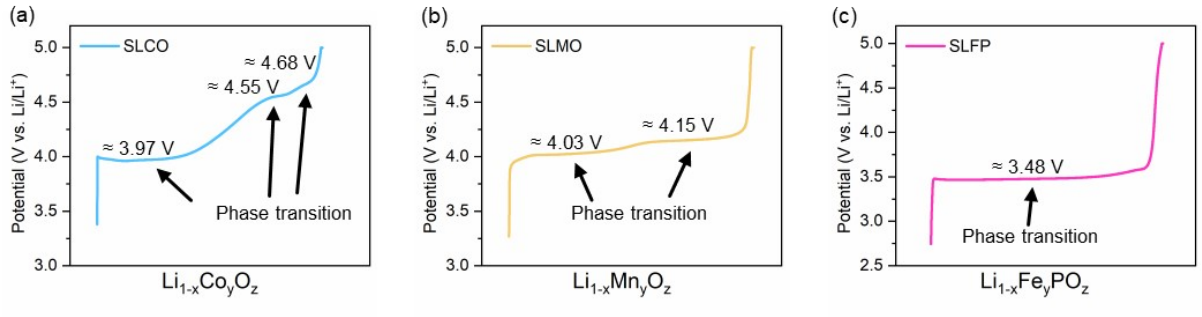

Fig. S1 Voltage profiles of SLCO, SLMO, and SLFP. The voltage profile of (a) SLCO showed three plateaus at ≈ 3.97 V, ≈ 4.55 V, and ≈ 4.68 V, (b) SLMO showed two plateaus at ≈ 4.03 V and ≈ 4.15 V, and (c) SLFP showed one plateau at ≈ 3.48 V. Plateaus indicate phase transition regions.

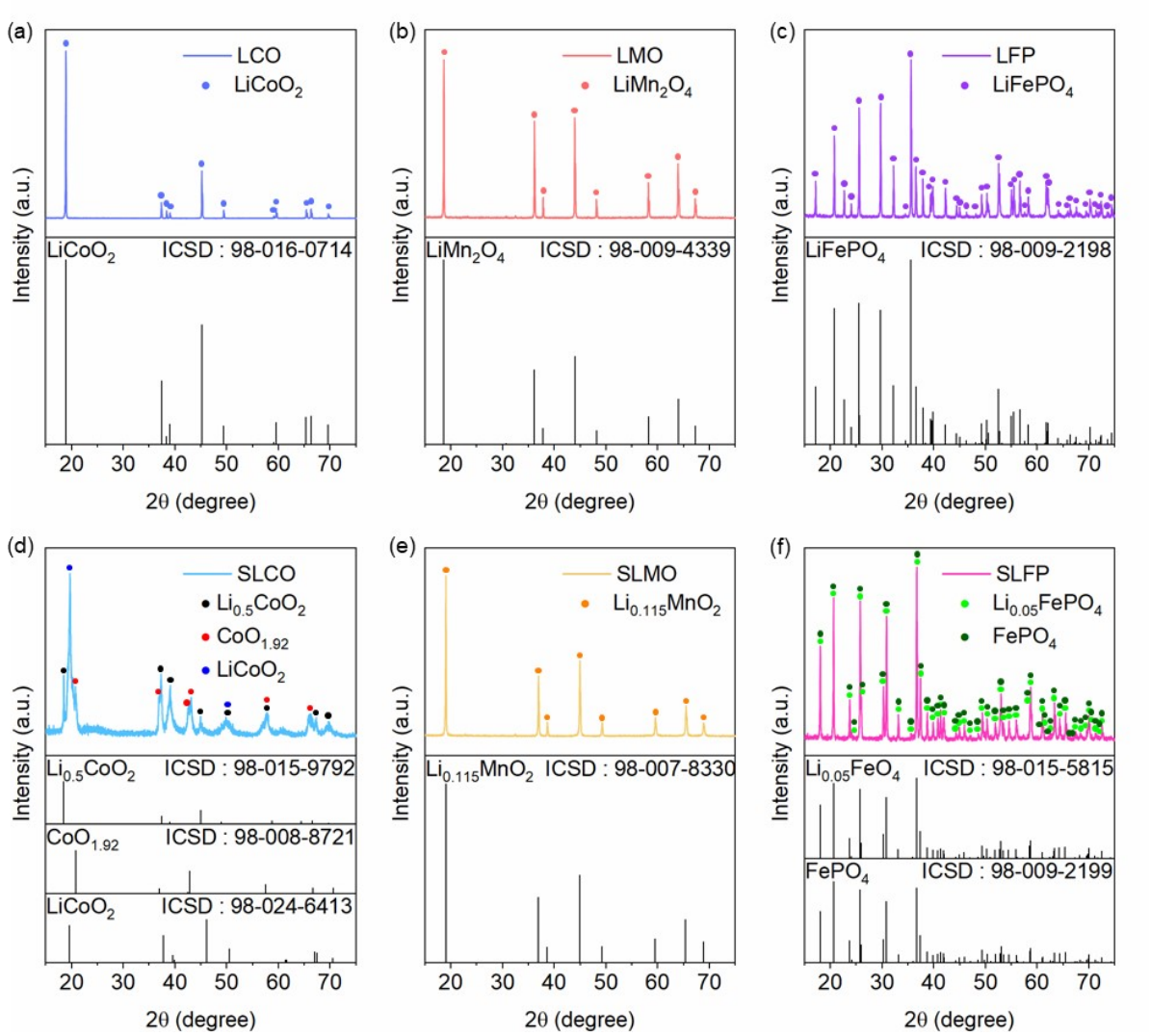

Fig. S2 XRD results before and after LiET. XRD patterns revealed different phases in each sample. Residual Li ions were observed.

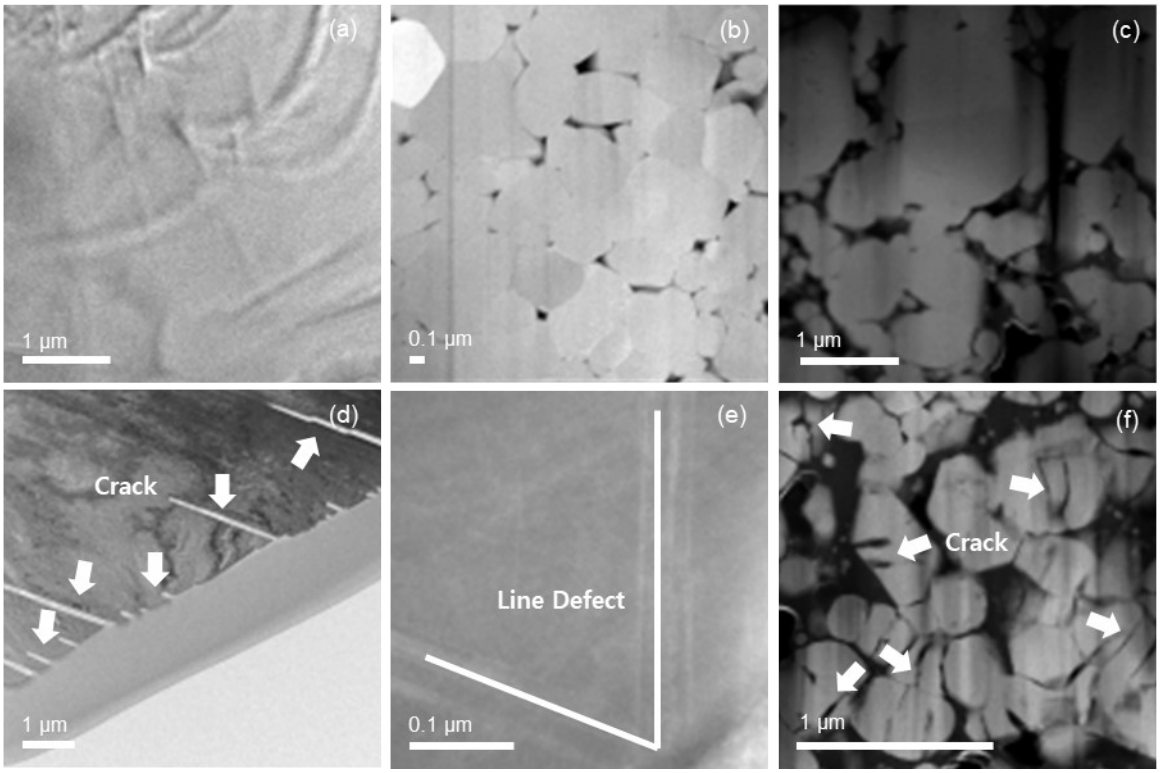

Fig. S3 TEM images of bulk–level for (a) LCO, (b) LMO, (c) LFP, (d) SLCO, (e) SLMO, and (f) SLFP. (a–c) LCO, LMO, and LFP showed intact states. (d and f) Cracks were observed in SLCO and SLFP. (e) Line Defects were discovered in SLMO.

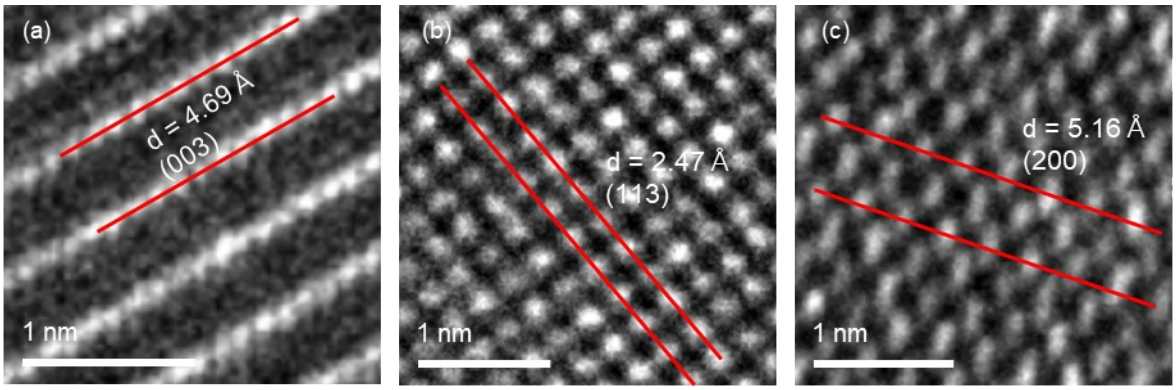

Fig. S4 HRTEM images of ordered atomic arrangements (a) $LiCoO_2$ indicated the (003) plane of $LiCoO_2$ with 4.69 Å spacing. (b) $LiMn_2O_4$ indicated the (113) plane of $LiMn_2O_4$ with 2.47 Å spacing. (c) $LiFePO_4$ indicated the (200) plane of $LiFePO_4$ with 5.16 Å spacing.

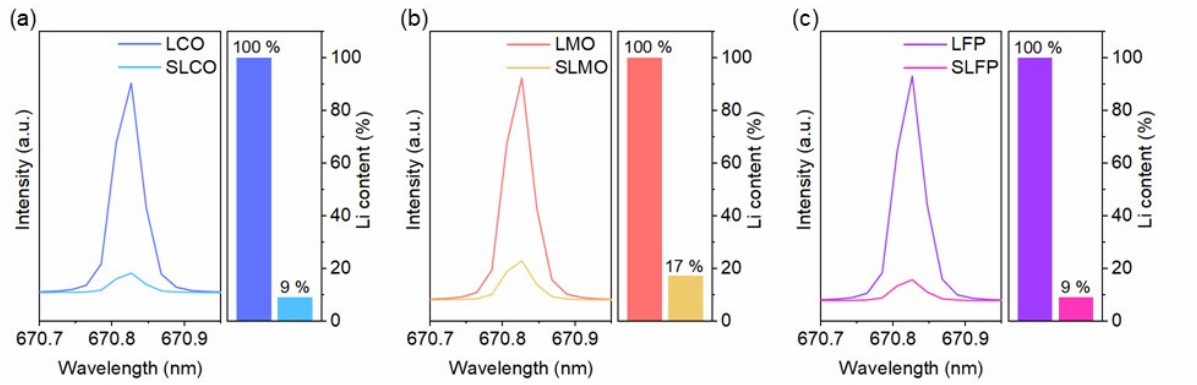

Fig. S5 ICP–OES analysis and comparative Li content (%) of (a) LCO and SLCO, (b) LMO and SLMO, and (c) LFP and SLFP. The remaining Li content of SLCO, SLMO, and SLFP presented in ICP–OES results corroborated the phases including a small amount of Li discovered in XRD results and the mixed–valent transition metal with a higher oxidation state revealed in XPS results.

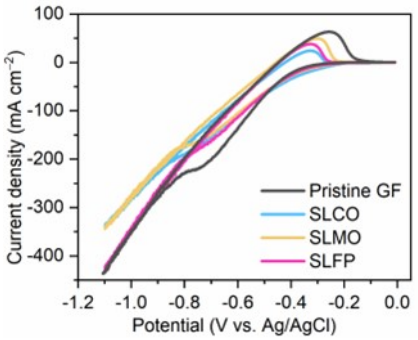

Fig. S6 Cyclic voltammetry curves of each material in 1 M V (III) + 3 M H_2SO_4 electrolyte.

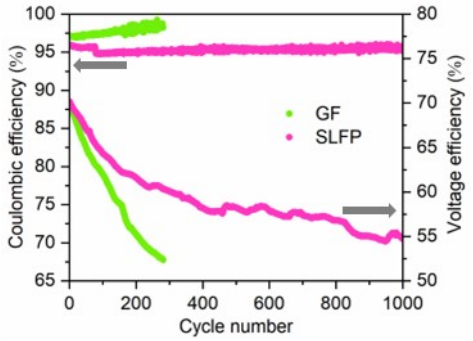

Fig. S7 Coulombic efficiencies and voltage efficiencies of GF (for 281 cycles) and SLFP (for 1000 cycles) at 300 mA cm^{-2}.

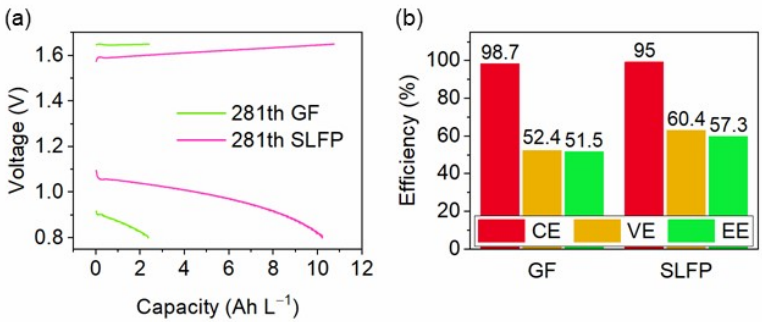

Fig. S8 Single cell performances of GF and SLFP operated at 300 mA cm^{-2}. (a) Charge−discharge curves during 281st cycle, (b) efficiencies after 281 cycles.

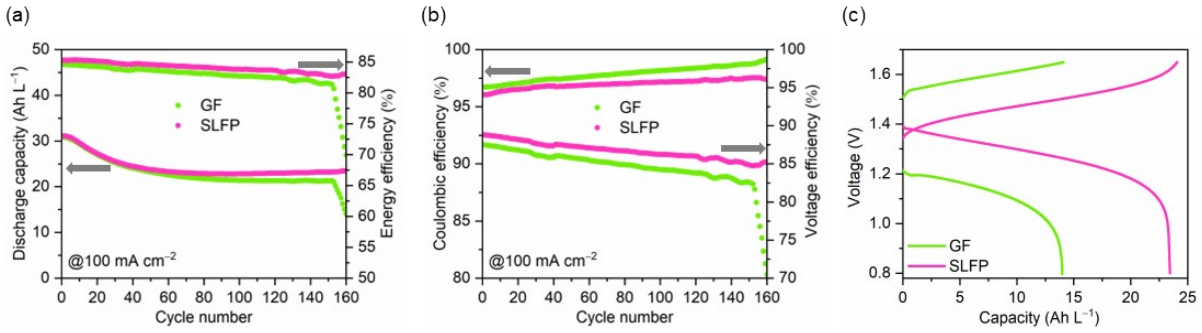

Fig. S9 Electrochemical performances of GF and SLFP in a VRFB single cell at a current density of 100 mA cm^{-2}. (a) Discharge capacity and energy efficiency of GF and SLFP. (b) Coulombic efficiency and voltage efficiency of GF and SLFP. (c) Voltage profiles during the 160th of GF and SLFP. From the 153rd cycle, a rapid degradation in electrochemical performances of GF was observed.

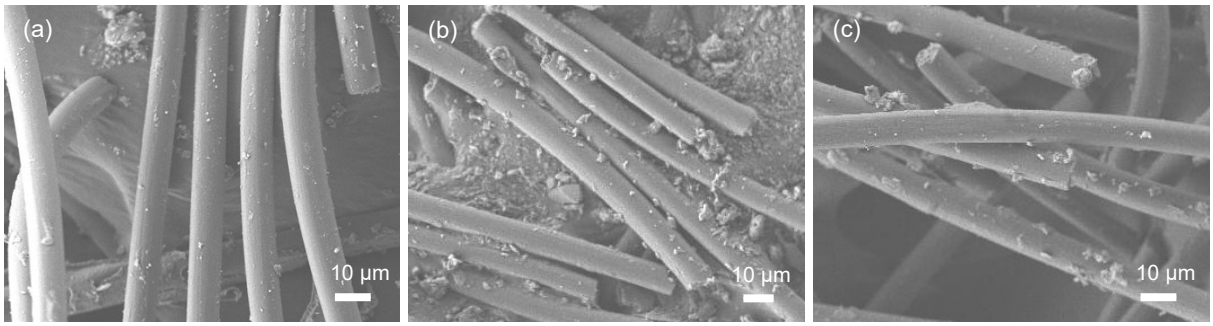

Fig. S10 SEM images of SLFP electrode before and after VRFB single cell test for 1000 cycles at a current density of 300 mA cm^{-2}. (a) SLFP electrode before 1000 cycles. (b) SLFP electrode on negative side after 1000 cycles. (c) SLFP electrode on positive side after 1000 cycles. There was no significant difference among these.

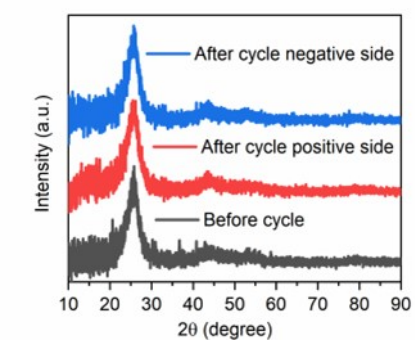

Fig. S11 XRD patterns of SLFP electrode before and after 1000 cycles in VRFB single cell test at a current density of 300 mA cm^{-2}. There was no significant difference among these.

Table S1 ΔE, R_s, and R_{ct} were listed in table. Relationship between ΔE and R_{ct} organized in increasing order

	SLFP	SLCO	LFP	SLMO	LCO	LMO	GF
Δ_E (V)	0.149	0.175	0.191	0.220	0.230	0.278	0.329
R_s (Ω cm^2)	1.09	1.08	1.10	1.10	1.10	1.11	1.12
R_{ct} (Ω cm^2)	3.52	4.11	4.19	5.50	7.99	10.13	22.04

Table S2 Variations in ΔE, R_{ct}, and O_2/O_1 before and after LiET.

	LFP–SLFP	LCO–SLCO	LMO–SLMO
ΔE (V)	0.042	0.055	0.058
R_{ct} (Ω cm^2)	0.67	3.88	4.63
O_2/O_1	15.56	2.10	0.67